Batteries & Supercaps

Research Article
doi.org/10.1002/batt.202400414

Chemistry Europe
European Chemical Societies Publishing

www.batteries-supercaps.org

Achieving High-Performance in Zinc Hybrid Capacitors with $Zn(TFSI)_2$/PEGDME Molecular Crowding Electrolytes

Nagaraj Patil,*[a] Diana Elena Ciurduc,[a] F. J. Landazábal,[a] and Rebeca Marcilla[a]

Aqueous Zinc-hybrid capacitors (ZHCs) are gaining attention for their high-safety, low cost, easy maintenance, high-power, and longevity. Despite various strategies to mitigate dendrites, corrosion, and HER, practical application remains challenging. Here, we utilize an advanced polyethylene glycol dimethyl ether (PEGDME)-based molecular crowding electrolyte (MCE) to significantly enhance performance of ZHCs. Our MCE offers a wider electrochemical stability window (2.7 V), low HER activity, and superior Zn anti-corrosion properties due to reduced water activity compared to conventional electrolyte. This results in higher coulombic efficiencies (98–100%) at various areal capacities and current densities, and longer longevity of Zn//Cu and Zn//Zn symmetric cells with MCE compared to conventional and water-in-salt electrolytes. The Zn/MCE/AC displays an enhanced voltage window (~2 V), achieving the highest capacitance (281 F/g), competitive energy density (138 Wh/kg), low self-discharge, and excellent cyclability (19100 cycles at 1 A/g with 100% capacity retention), indicating that MCE is a promising approach for practical energy storage applications.

Introduction

As the world continues to move towards renewable energy sources, such as solar and wind power, aqueous electrochemical energy storage systems (aq-EESs) will play an increasingly important role in storing this energy for use when it is needed.[1] In principle, the need for aq-EESs is driven by the demand for cost-effective, efficient, safe, and sustainable energy storage goals.[2] Aq-EESs are beneficial for multiple reasons. Firstly, they offer a safer and more environmentally friendly option compared to traditional non-aqueous electrochemical energy storage systems. The use of aqueous electrolytes reduces the risk of fire and explosion as they are less flammable than non-aqueous electrolytes.[3] Secondly, aq-EESs are generally more cost-effective than non-aqueous systems. Aqueous electrolytes are widely available and less expensive to obtain, whereas non-aqueous electrolytes can be costly, toxic and difficult to produce. This makes aq-EESs a viable economic option for large-scale energy storage, such as in grid-level energy storage systems.[4]

There are two main types of aq-EESs, i.e., conventional capacitors and batteries. Conventional capacitors, also known as electrochemical capacitors or supercapacitors, are energy storage devices that store electrical energy by separating positive and negative charges on the surface of two electrodes, typically made of carbons. On account of their fast kinetics and superb rate performance, they are generally applied in those devices that require high power output over a short period of time, such as in hybrid electric vehicles or in regenerative braking systems. The main drawback of conventional capacitors is their relatively low energy density compared to batteries, which means they cannot store as much energy per unit volume or mass. This limits their use in applications that require extended energy storage needs.

Conventional batteries that use aqueous electrolytes include lead-acid, nickel-cadmium/nickel-metal hydride, zinc/manganese dioxide, and zinc-ion batteries, etc. Although lead-acid batteries are widely used, they have low energy density and require high maintenance.[5] Nickel-based batteries have higher energy density but use toxic materials and have short cycle life.[6] Zinc/manganese dioxide batteries have higher energy density but lower power density,[7] while zinc-ion batteries with neutral electrolyte (e.g., $ZnSO_4$ aqueous solution) have received more attention, in which Zn anodes show an excellent stability.[8–10] Due to vast availability of different aqueous battery technologies, the choice of battery type depends on the specific application and requirements.[11–14]

Zinc metal anode, with high capacity of 823 mAh g^{-1} and low redox potential (−0.78 vs SHE),[9,15] are highly safe, low-cost, and environmentally friendly, and have been widely used in alkaline Zn/MnO_2 and Zn-air batteries.[16,17] However, Zn anode is known to suffer from poor service life in alkaline electrolyte due to dendrite growth and formation of insulating zinc oxide/hydroxide during use.[7,16,18]

Although the Zn anode shows improved plating and stripping reversibility in a neutral electrolyte compared to an alkaline electrolyte, the stability of the Zn anode in mild acidic electrolytes is still limited by several factors.[8,19–21] Dendrite growth during plating and stripping leads to safety issues, and undesired hydrogen evolution (H_2O decomposition) at the anode limits plating and stripping efficiency while increasing the local concentration of OH^- on the anode surface. The formation of $Zn(OH)_x$ on the anode surface converts dendritic Zn to electrochemically inert 'dead' Zn, which limits efficient Zn utilization. When it comes to the performance of Zn-ion

[a] Dr. N. Patil, Dr. D. E. Ciurduc, F. J. Landazábal, Dr. R. Marcilla
Electrochemical Processes Unit, IMDEA Energy Institute, Avda. Ramón de la Sagra 3, Móstoles, 28935, Spain
E-mail: nagaraj.patil@imdea.org

Supporting information for this article is available on the WWW under https://doi.org/10.1002/batt.202400414

batteries, the cyclability and rate performance are often limited by conventional battery-type cathodes.

Zinc hybrid capacitors (ZHCs) use a combination of capacitive cathode and battery-type anode (Zn) to achieve high energy (higher than conventional supercapacitors) and power (higher than conventional Zn-ion batteries) densities.[22,23] Despite their good compromise between anticipated energy and power density, the ZHCs still face several limitations in terms of performance of the full device. One limitation is the need for a suitable cathode material that can provide high capacity and high power density. Another limitation is the need for a suitable electrolyte that can provide good ionic conductivity and high stability over many charge/discharge cycles.[24] In principle, ZHCs have great potential as a new type of energy storage system, but further research is needed to address the limitations and improve their overall performance.

The use of conventional alkaline electrolytes results in a low coulombic efficiency of about 50% due to the formation of zinc by-products.[21] Zinc anodes are also prone to dendrite growth, and while mild/neutral electrolytes can help reduce it, the coulombic efficiency during Zn plating/stripping remains unsatisfactory (around 70%), as well as the formation of $Zn_4SO_4(OH)_6{\bullet}5H_2O$ by-products.[25] To improve the energy storing capacity and stability, concentrated electrolytes with $ZnSO_4$, $ZnCl_2$, and $Zn(CH_3COO)_2$ salts have been used but with limited improvement in cycling stability.

Water-in-salt electrolytes (WiSE) have been used to enhance the reversibility of Zn metal negative electrodes. WiSE possess a larger electrochemical stability window compared to diluted solutions and enable enhanced reversibility of the Zn anode due to the limited amount of free water molecules.[26] Some examples of WiSEs are 30 m $ZnCl_2$,[27,28] 1 m $Zn(TFSI)_2$ + 20 m LiTFSI,[21] and the concentrated urea/$Li(TFSI)_2$/$Zn(TFSI)_2$ mixture,[29] which have resulted in excellent plating/stripping performance of Zn anodes, offering high coulombic efficiencies (95.4%, 99.9%, and 96.0%, respectively). Recently, low-cost and halide-free WiSE based on high-concentration acetate solutions have emerged, and a Zn-containing acetate WiSE has been developed for ZHC that addressed the unsatisfactory cycling stability of the Zn cells mentioned above.[30]

Lately, molecular crowding electrolytes (MCEs) have shown great promise in the development of advanced energy storage systems, such as Li-ion, Zn-ion batteries and capacitors.[31–33] Particularly, in the previous generation MCEs for ZIBs, PEG400 (PEG stands for polyethylene glycol) was used as molecular crowding agent, while in this work, we changed to PEGDME450 (PEGDME denotes polyethylene glycol dimethyl ether) serves the same purpose, is mainly due to their different molecular weights and properties. PEGDME450 has a larger molecular weight than PEG400, which means that it can occupy a larger space and create more molecular crowding.[34] In addition, PEGDME450 has better solubility in high-voltage electrolytes compared to PEG400, which can result in better stability and longer cycle life of the energy storage device. Furthermore, PEGDME450 has a lower viscosity than PEG400, which can facilitate the ion transport in the electrolyte and reduce the resistance of the energy storage device.[34] These factors make PEGDME450 a more suitable molecular crowding agent for high-performance energy storage devices.

Activated carbon (AC) has been commonly used as an electrode material for ZHCs, as reported in various studies.[35,36] AC has a high surface area and high electrical conductivity, enabling it to store large amounts of charge and improve the overall energy density of the device. In addition, AC is low-cost, abundant, and environmentally friendly. However, AC-based electrodes in ZHCs have a few drawbacks. Firstly, these electrodes require a binder, conductive additive, and metal current collector, which increases the total weight of the device and consequently reduces its final energy density. Secondly, AC-based electrodes that use the energy storage mechanism of electrochemical double-layer capacitors have limited capacities. Hence, there is a need to develop new types of capacitor electrodes that do not require binders or conductive additives.

Buckypaper, a thin film made of carbon nanotubes, has been widely used as an electrode material in various energy storage devices due to its unique properties, such as high surface area, mechanical flexibility, and electrical conductivity.[37] Recently, there have been studies on using AC as the active material in buckypaper electrodes for energy storage applications.[38] The combination of buckypaper and AC has shown promising results in terms of high specific capacitance, good cycling stability, and excellent rate capability. Moreover, the use of carbon nanotubes eliminates the need for a binder and conductive additives, which reduces the weight and simplifies the fabrication process of the electrodes. Therefore, buckypaper with AC as the active-material has great potential in developing high-performance energy storage devices.

The main objective of this work is to improve the performance of ZHCs by increasing their lifespan and capacitance. Higher capacitance is achieved by maximizing the voltage window of the ZHCs, and improved lifespan can be achieved by using a MCE and an AC-based buckypaper cathode. This approach offers several advantages, such as low cost and high sustainability, making it an attractive alternative to traditional batteries and supercapacitors. Specifically, in this work we compare the properties of Zn electrolytes, stability and compatibility Zn anode and performance of Zn//AC ZHCs in our MCE composed of 1 m $Zn(TFSI)_2$ in 85/15 PEGDME450/H_2O (acronymed as MCE from here onwards) with a conventional electrolytes, 1 m $Zn(TFSI)_2$ that lacks the crowding agent (acronymed as CE from here onwards) and a widely used WiSE composed by 1 m $Zn(TFSI)_2$ + 20 m LiTFSI (acronymed as WiSE from here onwards).The use of MCE has been shown to improve the reversibility of Zn metal negative electrodes, resulting in better plating/stripping performance and higher coulombic efficiency compared with WiSE and CE. The physico-chemical, ion-transport, and structural properties of these electrolytes were studied. Detailed investigations were conducted on anode corrosion and Zn plating/stripping behavior, and the electrochemical performance of full cells in terms of capacity, rate capability, cycle stability and self-discharge characteristics were assessed. The newly developed MCE showed superior performance metrics, particularly cycle life and anti-self-discharge characteristics compared to the other electrolytes.

Research Article
doi.org/10.1002/batt.202400414
Chemistry Europe
European Chemical Societies Publishing

Results and Discussion

Different Aqueous Electrolyte Formulations, Ion-Transport and Physico-Chemical Properties

Ion Transport Properties. Initially, we assessed the ionic conductivity (σ), Zn^{2+} transport number (t_{Zn}^{2+}), and electrochemical stability window of the formulated CE and MCEs. In Figure S1a, the σ of the electrolytes is depicted as a function of PEGDME450 concentration at 25 °C. The results indicate that the σ of the PEGDME-based electrolytes decreases as the weight fraction of crowding agent (PEGDME450) increases from 50 to 94% of, as expected.[31,32,34] It can be observed that the σ varies between 5.61 to 0.50 mS cm^{-1} in the mentioned range. Due to its visibly lower viscosity (not measured),[34] the PEGDME450 MCE displays conductivity that is 4.6 times higher (5.6 mS cm^{-1}) than that of the traditional PEG400 MCE (1.23 mS cm^{-1}; both are 1 m $Zn(TFSI_2)$-50% crowding agent-50% H_2O).[32] Notably, the σ value for the CE is 28.88 mS cm^{-1}, while the WiSE presented a σ of 36.88 mS cm^{-1}, which are clearly higher than that of the MCEs. In Figure S1b, the Nyquist impedance plots of both the CE and MCEs are presented. The plot showcases a semicircle arc in the high-frequency range, accompanied by a spike in the low-frequency range. The semicircle arc illustrates the resistive and capacitive properties of the electrolyte, while the spike represents the non-ideal interfacial capacitance at the electrolyte–electrode interface. By determining the intercept of the semicircle on the real axis, the resistance (R_b) can be calculated. With the increase of PEGDME450 concentration, the bulk resistance of the MCEs increases. On the other hand, the CE exhibits the lowest resistance value, indicating that its RT ionic conductivity is the highest.

MCEs based on PEGDME exhibit higher t_{Zn}^{2+} values (ranging from 0.40 to 0.88) in comparison to the conventional diluted electrolyte (CE; with a t_{Zn}^{2+} of only 0.1, as demonstrated in Figure S2. As expected, the t_{Zn}^{2+} value increases as the PEGDME concentration increases, and the 1 m $Zn(TFSI)_2$ – 94:6 wt% PEGDME/H_2O electrolyte shows a maximum value of 0.88.

Based on its high σ (1.47 mS cm^{-1}), and competitive t_{Zn}^{2+} (0.87), the electrolyte with 85:15 wt% PEGDME/H_2O (this particular electrolyte here onwards referred as MCE) was identified as the most promising option. Therefore, the subsequent sections focus on the detailed investigation of this optimized molecular crowding electrolyte and its potential suitability for use in aqueous Zn//AC hybrid devices.

Electrochemical Stability Window. We use linear sweep voltammetry (LSV) to evaluate the voltage window of aqueous electrolytes (Figure 1). The increased electrochemical stability of water owing to the presence of ethereal oxygen atoms (and the associated strong H_2O-crowding agent interactions) in the crowding agents was also confirmed in our results, in accordance with the previous studies.[34] The ESW of the MCE was found to be approximately 2.7 V, which is at least 0.27 V higher than that of CE lacking PEGDME. The OER inflection point for MCE on the anodic side showed +0.2 V positive shift compared to the CE. On the cathodic side, two competing reactions are likely taking place simultaneously: Zn^{2+} deposition and HER. Thus, a real onset potential for HER cannot be assessed, but a negative shift of onset potential for reduction reactions was evident for MCE. Additionally, current density for both OER and HER processes in MCE evidently decreased with the use of PEGDME, being much lower compared to that in the CE.

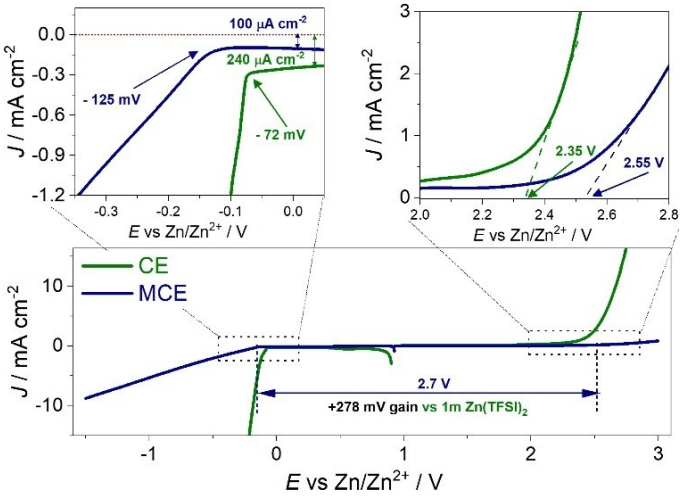

Figure 1. The electrochemical stability window, determined by LSV in a three electrode cell (Pt as working, Zn as counter and reference electrodes).

In addition, Tafel analysis demonstrated that MCE had higher Tafel slope compared to CE (as shown in Figure S3), indicating that it has slower kinetics towards undesired cathodic reactions. It is important to note that in these experiments, a platinum disc was used as the working electrode, which is a catalyzer for HER reactions. However, in the actual battery with a Zn metal anode, we expect that the HER would be lower due to the higher overpotential of the Zn metal for HER.

Raman Spectroscopy. To investigate the ion environment of these aqueous electrolytes, Raman spectroscopy was used (Figure S4). The first region, spanning from 3100–3700 cm^{-1} (Figure S4a), is associated with the characteristic O–H stretching bands of water molecules, which can be differentiated into strong (~3230 cm^{-1}), weak (~3350 cm^{-1}), and non H-bonded (~3560 cm^{-1}) types.[39,40] The Raman spectrum of the CE shows a broad band with three peaks, which correspond to different types of water molecules.[41] The addition of PEGDME results in an increase in the peak of non H-bonded water molecules at 3547 cm^{-1} with simultaneous decrease in the intensity of the peak at 3200 cm^{-1}, associated with strong water-water interactions, indicating that the water molecules are trapped by PEGDME. Therefore, on the grounds of our previous literature reports, and supplemented by others as well,[34] in the context of crowding phenomenon, we can reasonably conclude that that the fraction of "free water" molecules in the MCE were significantly reduced with an effective gain of non-hydrogen bonded and single hydrogen bonded water molecules at the expense of fully hydrogen bonded water in tetrahedral complexes.[42]

Research Article
doi.org/10.1002/batt.202400414
Chemistry Europe
European Chemical Societies Publishing

Characterization of Zn Metal Anode

Corrosion of Zn Foils. Zinc metal corrodes very slowly in neutral aqueous solutions, but the corrosion process is accelerated in most conventional Zn-based aqueous electrolytes that are mildly acidic (pH 3.6–6.0).[43,44] To investigate the stability of Zn metal in PEGDME-MCE and CE, we immersed commercial Zn foil in the respective aqueous solutions. After 21 days, FE-SEM images revealed that the Zn metal was uneven and covered with large and irregular by-products, in the case of the CE. In contrast, in our MCE, the distribution of by-products was almost imperceptible and very uniform. (see Figure S5). Energy-dispersive X-ray spectroscopy (EDS) (Figure S6 and S7) confirms that the solid deposits were made of Zn, Carbon, Oxygen, Fluorine and Sulphur elements. Additionally, X-ray diffraction (XRD) showed the formation of various crystalline by-products, such as $Zn(OH)_2$, $xZnCO_3yZn(OH)_2zH_2O$, and ZnO when the Zn foil was immersed in the CE. In contrast, these crystalline by-products were almost absent in our MCE (see Figure S8).[45]

Assessment of Zn Plating/Striping Reactions by CV. Figure 2a shows the results of the investigation into the reversibility of Zn plating/stripping using cyclic voltammetry (CV). Both electrolytes demonstrated a reversible electrochemical stripping/plating process of Zn with an enhanced coulombic efficiency (CE) of 98% for MCE compared to a lower 67% for the CE.

Assessment of Zn Plating/Striping Reactions in Zn//Cu Cells. To assess the reversibility of Zn plating/stripping, Zn//Cu asymmetric cells were assembled and tested under various conditions. Initially, we kept the areal current at 1 mA cm^{-2} and tested the asymmetrical cells at variable areal capacities ranging from 0.2 to 10 mAh cm^{-2} (Figure 2b, Figure S9). Zn//Cu cells in the MCE displayed excellent coulombic efficiencies mostly in the range of 98–100%, with an impressive value of >99% even at high areal capacity of 10 mAh cm^{-2}. In contrast, the coulombic efficiencies of Zn//Cu cells in the CE did not exceed 95% even under less severe conditions and exhibited a drastic drop in the coulombic efficiency values at higher areal capacities (see capacity-voltage profiles in Figure S9b–d). Note that from here onwards we have included another reference electrolyte, i.e., water-in-salt (WiSE; composed by 1 m $Zn(TFSI)_2$ and 20 m LiTFSI in H_2O) to compare the performance. Also

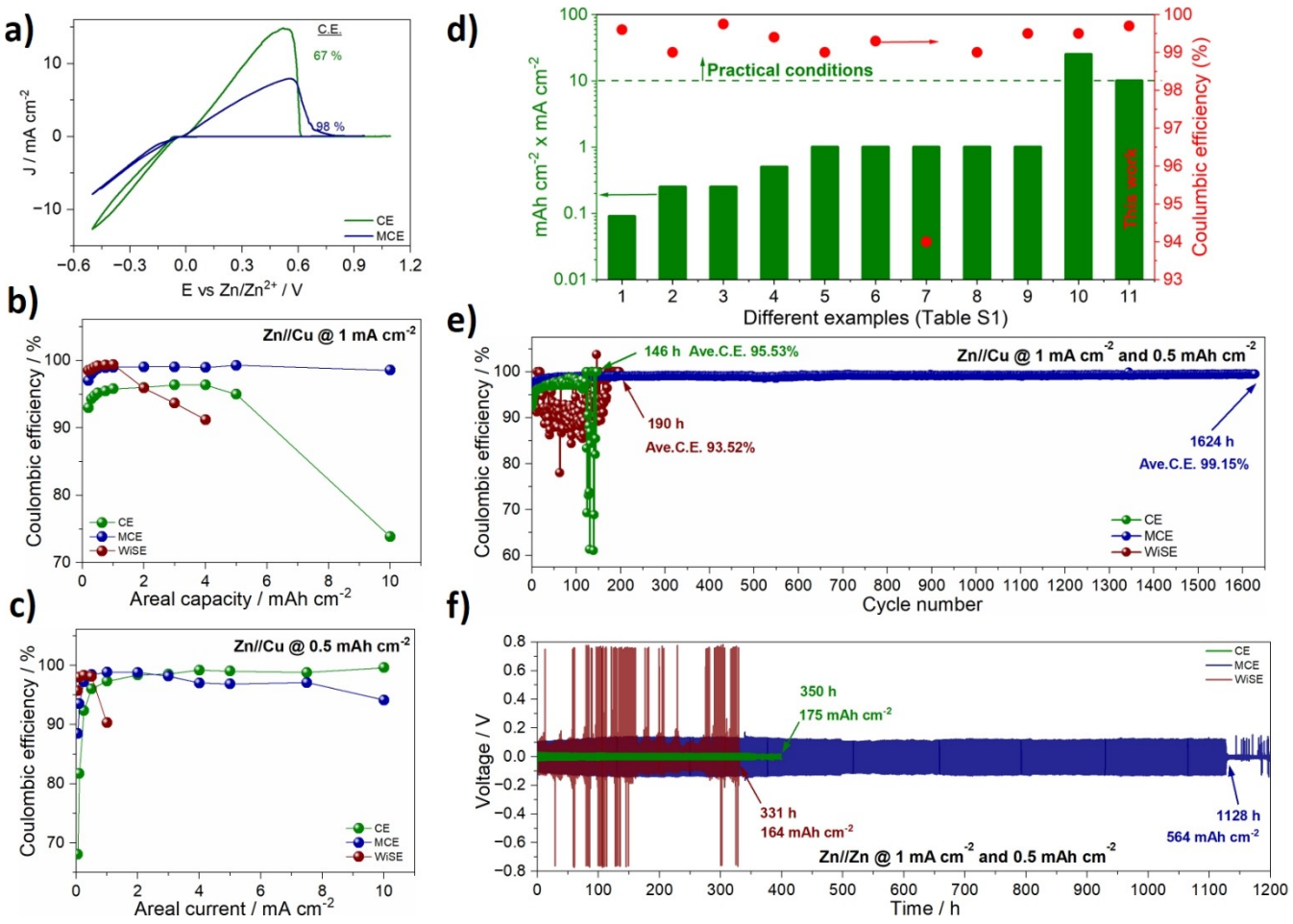

Figure 2. (a) Cyclic voltammograms at 1 mV s^{-1} in three-electrode configuration for electrolytes CE and MCE. The current intensity for CE was divided by 150-factor for better visualization. Coulombic efficiencies of Zn//Cu asymmetrical cells at different areal capacities and at a fixed areal current of 1 mA cm^{-2} (b), and at different areal currents and at fixed areal capacity of 0.5 mAh cm^{-2} (c). (d) Coulombic efficiencies of Zn//Cu asymmetrical cells upon long cycling at 1 mA cm^{-2} and 0.05 mAh cm^{-2}. (e) Top range: Zn plating/stripping in Zn//Zn symmetrical cell at 1 mA cm^{-2} and 0.5 mAh cm^{-2}, and bottom range: different periods of time are zoomed.

Research Article
doi.org/10.1002/batt.202400414
Chemistry Europe
European Chemical Societies Publishing

notably, the WiSE exhibited good coulombic efficiencies around 99% only at the lower areal capacities (below 2 mAh cm^{-2}), while they dropped below 95% until 4 mAh cm^{-2}, and the cell was non-operational beyond 4 mAh cm^{-2}, inferring superiority of our MCE over CE and WiSE for practically relevant areal capacity conditions.

Next, we maintained a fixed areal capacity of 0.5 mAh cm^{-2} and varied the current density from 0.05 to 10 mA cm^{-2} (Figure 2c, Figure S10). The coulombic efficiencies were consistently higher in our MCE compared to the CE until 0.5 mA cm^{-2}, indicating that our molecular crowding electrolyte minimizes parasitic reactions (mostly HER) in the low areal current regime. In the intermediate areal current range between 1–3 mA cm^{-2}, the coulombic efficiencies for MCE and CE were comparable, and in the high areal current regime, the trend was inverted, probably due to the higher ionic conductivity and associated enhanced transport properties with fast kinetics that reflected in lower overpotentials as evidenced by the areal capacity-voltage profiles (Figure S10b–d) in the CE. On the contrary, the WiSE showed coulombic efficiencies around 98% until 0.5 mA cm^{-2}, then a sudden drop in the values and a short circuit was observed. These results once again showcase superiority of our MCE over CE, particularly at low areal current and over WiSE, particularly at high areal current regimes, respectively.

We preliminarily compared the coulombic efficiency of our MCE with the relevant state-of-the-art (see Table S1). As shown in Figure 2d, our MCE not only archives practically-relevant capacities and currents ($\geq$10 mAh cm^{-2}×mA cm^{-2}), but also exhibits quantitative coulombic efficiencies (>99.7%) compared to the state-of-the-art.

Figure 2e and Figure S11 illustrates the long-term cycling performance of Zn//Cu cells, which remained stable for 1624 hours with average coulombic efficiency around 99.2% in our MCE. Under the same conditions, the CE exhibited a moderate average coulombic efficiency of 95.5% and experienced cell failure after only 146 hours. The WiSE presented an average Coulombic efficiency of 93.5% and a short circuit after 190 hours. These results indicate that our MCE significantly reduces parasitic reactions, such as HER, and enables almost complete recovery of the deposited Zn on copper during subsequent stripping processes.

FE-SEM was utilized to examine the surface morphology of Zn and copper electrodes after 15 plating/stripping cycles in a Zn//Cu cell. The stripped Zn surface showed a more uniform stripping with our MCE, while a non-uniform stripping with corrosion pits was observed both in the CE and WiSE (Figure 3a, Figure S12). Porous, mossy, non-homogeneous and dendritic Zn deposits on Cu were observed in both the CE and WiSE (Figure 3b, Figure S13). However optimistically, a near ideal and

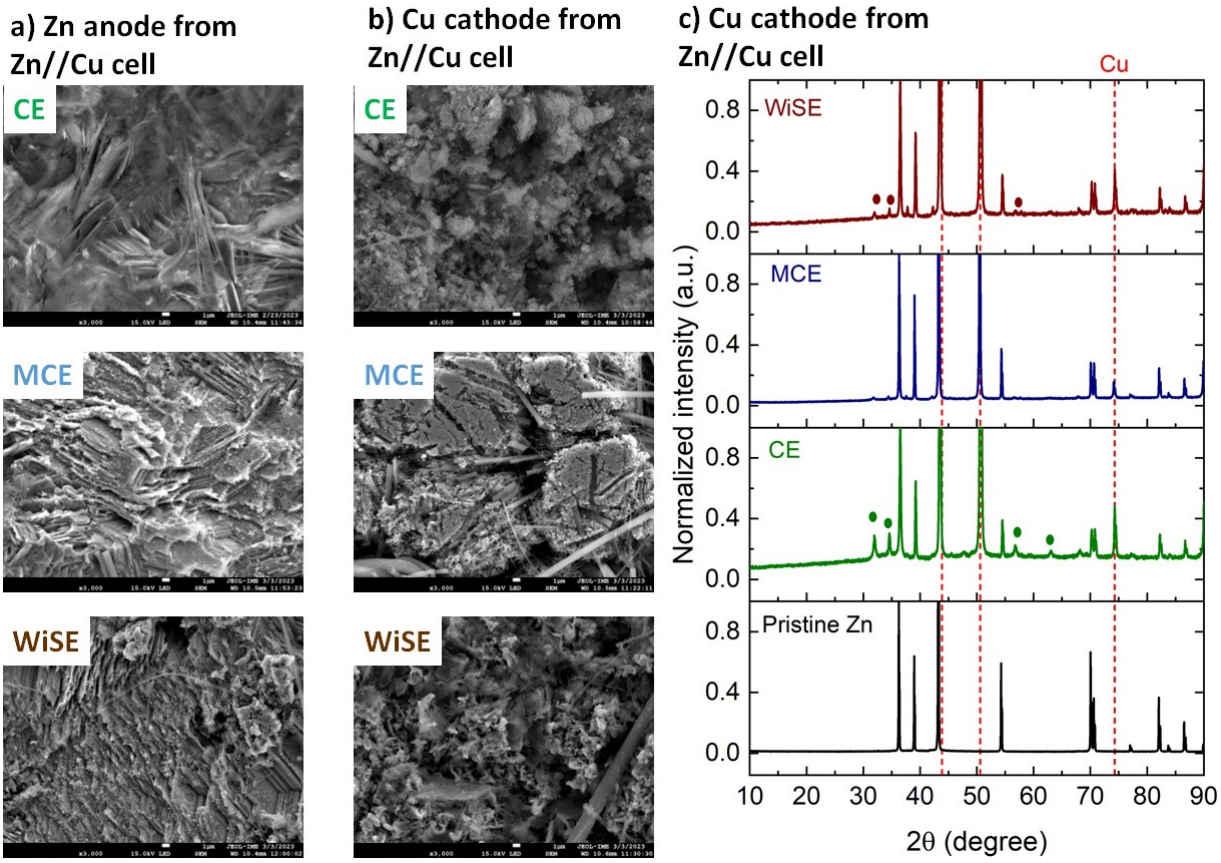

Figure 3. Surface morphology of stripped Zn anode (a) and plated Zn on Cu (b) by FE-SEM in a Zn//Cu cell at 1 mA cm^{-2} with the discharge/charge capacity of 3 mAh cm^{-2} after 15 cycles in CE, MCE and WiSE. Scare bar and magnification is 10 μm and x3000, respectively. c) Characteristic XRD pattern of Zn depositions on Cu. The dashed lines in a correspond to the Cu substrate diffraction peaks. The filled circles indicate the diffraction peaks correspond to the zincate and hydroxide by-products.

Research Article
doi.org/10.1002/batt.202400414
Chemistry Europe
European Chemical Societies Publishing

more homogeneous deposition of Zn was observed with our MCE. EDS (Figure S14-S16) confirmed that the solid deposits were made of Zn, carbon, oxygen, fluorine, and sulfur elements with a relatively larger proportion of Zn (compared to Cu) and a smaller proportion of O and C (compared to Zn) in both MCE and WiSE, indicating better uniformity of the plated Zn and less zincates population, respectively. Additionally, similar conclusions can be drawn from the EDS analyses of the stripped Zn anodes, revealing less zincates population (the smaller proportion of O and C compared to Zn) in both MCE and WiSE compared to the CE (Figure S17–S19). Moreover, the XRD of the plated Zn on the Cu cathode (Figure 3c) and stripped Zn anode (Figure S20) in the CE and WiSE showed additional peaks, which correspond to the zincate and hydroxide by-products. In contrast, Zn and copper substrates were mostly free of these by-products in our MCE

Assessment of Zn Plating/Striping Reactions in Zn//Zn Cells. The performance of these electrolytes in relation to the Zn semi-reaction was analyzed in symmetric Zn//Zn cells that were galvanostatically cycled at 1 mA cm^{-2} and 0.5 mAh cm^{-2}. The MCE exhibited higher viscosity and lower ionic conductivity, resulting in an average voltage polarization of about 280 mV in MCE, while the CE displayed only 40 mV. However, cell failure occurred prematurely after 350 hours of cycling in the latter electrolyte, while the former sustained up to 1128 hours before an internal short circuit occurred (Figure 2f). Furthermore, the cycling of Zn//Zn in WiSE was not satisfactory, resulting in undesired voltage fluctuations, non-quantitative coulombic efficiencies that led to cell failure after 331 hours of operation. The growth of Zn dendrites, resulting from the irregular deposition on the Zn anode and possibly penetrating the separator to cause short-circuits, is most likely led to the cell failure, which was substantially delayed with our MCE.

In summary, these findings indicate that our optimized MCE displays enhanced ESW, especially on the anodic side, with higher reversibility of Zn plating/stripping and a smoother Zn deposition/removal process than the CE. This improvement, which is attributed to the PEGDME-mediated reduced water activity as determined also by Raman spectroscopy, and better kinetics of Zn plating/stripping reactions compared to the WiSE are expected to significantly enhance the performance of Zn// AC devices under practically relevant conditions.

Assembly and Testing of Zn//AC Device

Working Principle. Typically, the devices are utilized with a two-electrode setup in practical applications. In order to determine the maximum available operating voltage, tests were performed using a coin cell configuration with AC buckypaper electrode serving as the cathode, zinc foil as the anode, and CE, MCE or WiSE as the electrolytes (see Figure 4a for the schematic of the cell). This Zn//AC hybrid device (ZHC) is sought to work on the principle of reversible electrochemical reactions of Zn^{2+} plating/stripping on the zinc (Zn) anode and adsorption/desorption of anions on the activated carbon (AC) cathode, within an approx. voltage window of 2 V (Figure 4b).[36] During charging,

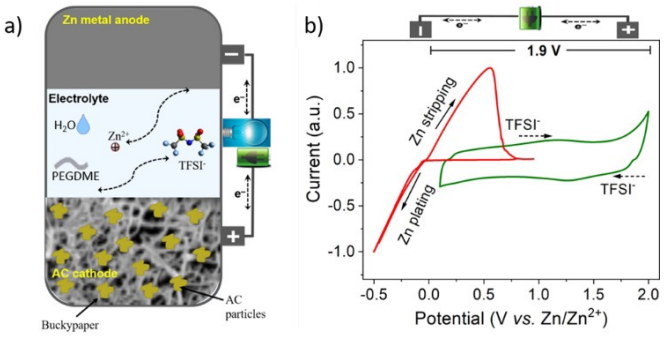

Figure 4. (a) Schematic illustration of Zn//AC hybrid capacitor, and (b) CV curves of the Zn anode and the AC cathode in MCE at a scan rate of 1 mV s^{-1}.

the Zn anode undergoes reduction reaction with the plating of zinc ions from the electrolyte, while the AC cathode, which has a high surface area due to its porous structure, stores the anions on its surface at the same time, electrons are released from the AC cathode and travel through the external circuit to the Zn anode, where they are stored. This process results in the charging of the device and the storage of electrical energy. During discharging, the process is reversed. The Zn anode undergo stripping process with the release of zinc ions into the electrolyte, while anions being desorbed from the AC cathode. The electrons travel through the external circuit, providing a flow of electrical current that can be used to power a device or recharge another battery.

Optimization of Voltage Window. First, the operating voltage was assessed using CV across various voltage ranges, as shown in Figure 5a. The CV curves maintained a quasi-rectangular shape between 0.2 V and 1–1.8 V in all electrolytes. However, increasing the upper cut-off voltage to and beyond 1.9 V resulted in a notable increase in current response at higher voltages due to oxygen evolution reactions (OER) in CE. In contrast, for MCE and WiSE, there was no notable increase in current at higher voltages up to 2.2 V.

Nanoporous carbon materials, especially those with numerous defects, can undergo electrochemical oxidation at higher voltages, leading to the generation of surface oxides such as carboxyl and carbonyl.[46,47] These surface groups can contribute to pseudocapacitive faradic redox charge storage, creating dormant redox peaks in the CV. However, the presence of such groups is minimal in MCE and WiSE compared to CE. These carbon oxidation processes can occur before OER, limiting the highest operating voltage for carbon-based electrodes. Although the device can function beyond the maximum voltage range, its cycle life and safety are significantly compromised.

The electrochemical voltage window of the ZHCs was examined in greater detail using galvanostatic charge-discharge (GCD) at a current density of 1 A g^{-1}, as depicted in Figure 5b. When the voltage remained below 1.8 V, the charge-discharge curves exhibited high symmetry, indicating typical capacitive behavior. However, once again as the voltage raised to and beyond 1.9 V, the charge curve's linearity was not maintained at

Research Article
doi.org/10.1002/batt.202400414
Chemistry Europe
European Chemical Societies Publishing

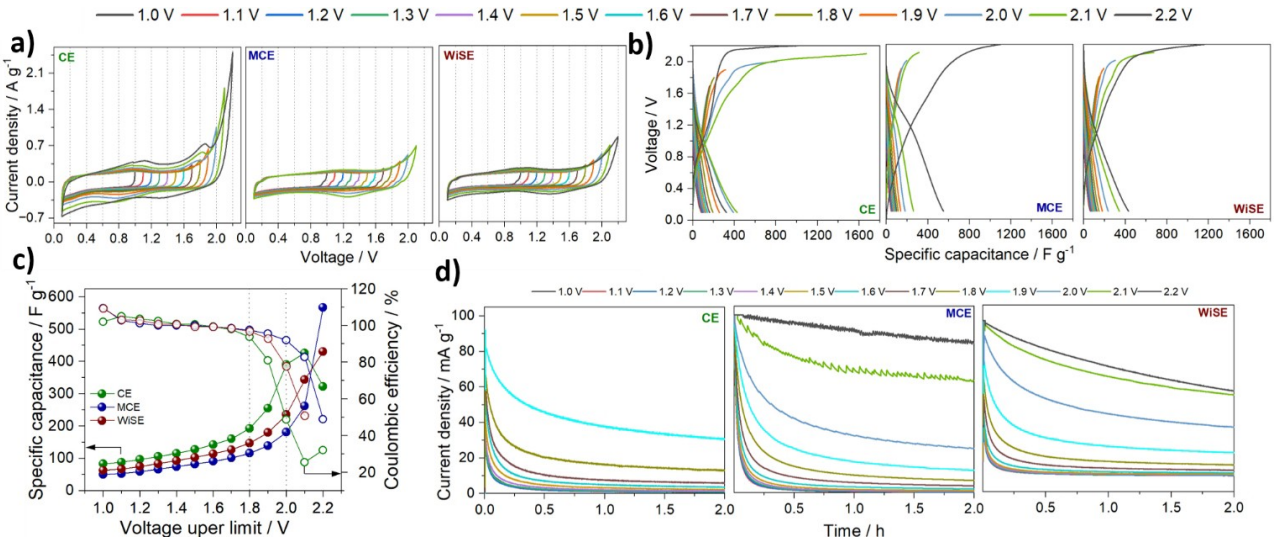

Figure 5. Voltage window optimization of ZHCs with CE, MCE and WiSE. Cyclic voltammograms at 1 mV s^{-1} (a) and GCD voltage-specific capacitance profiles at 1 A g^{-1} with stepwise increase in upper cell voltage limit (b), and the corresponding specific capacitances and coulombic efficiencies at different voltage ranges (c). d) Leakage current profiles upon potentiostatic aging at various upper voltage cut-off limits.

the higher voltage ranges due to the oxidation of carbon surface groups in the CE, and similar observations were also made for ZHC in WiSE above 2 V, while in the MCE, the good symmetry is maintained till 2.1 V. These findings are largely consistent with the CV results.

Furthermore, Figure 5c shows the evolution of coulombic efficiencies and specific capacitances calculated for different voltages by GCD experiments. The coulombic efficiency is determined by dividing the discharge capacitance by the charge capacitance. Generally, the ZHCs exhibit excellent charge and discharge reversibility with near-quantitative coulombic efficiencies of 98–100% in the voltage range between 0.2 V to 1.8 V for both the MCE and WiSE. On the contrary, when CE is used, the coulombic efficiency doesn't exceed 93% at 1.8 V of voltage upper limit. However, when the voltage exceeds 1.9 V, the order of coulombic efficiency decay was CE > WiSE > MCE. For instance, at a voltage upper limit of 2 V, a higher coulombic efficiency of 92% was attained in MCE compared to lower 77 and 49% in WiSE and CE, respectively. A coulombic efficiency below 100% indicates the occurrence of irreversible reactions during the charging process at high voltages. Additionally, contrast to a conventional battery or a traditional symmetric capacitor, the specific capacitance of ZHCs evolved increasingly with the increment of voltage range in CE > WiSE > MCE order till 2.1 V.

Although the CV and GCD tests can detect the onset of side reactions, it is challenging to identify the reaction immediately when it is kinetically controlled, but thermodynamically feasible. Thus, the electrochemical voltage window of the ZHCs was further investigated using a combination of GCD and potentiostatic aging. In this test, the cell was charged to a set voltage upper limit and maintained at that voltage for 2 h to observe the leakage current response before being discharged (Figure S21). The final dwell current (termed as leakage current, i_{leak}) response during the potentiostatic aging was used to evaluate the cathode stability. If the final dwell current is negligible, it indicates ideal electric double-layer behavior, free from parasitic reactions such as HER/OER with insignificant faradaic contributions.[48] The computed i_{leak} are collected in Table S2, and the corresponding current-time profiles showed in Figure 5d. In the voltage range between 0.2 to 1.7 V, the final current response was close to zero during the dwell period, indicating the ideal electric double-layer behavior. However, at 1.8 and 1.9 V voltage upper limits, the i_{leak} were much higher than zero particularly in CE, and were almost 1.9- and 2.4-fold higher than that in MCE, suggesting a slow pseudocapacitive current under these voltage regimes. Moreover, for CE at 2 V, the failure of the cell under this high voltage was occurred probably because of drastic faradaic reactions, identified with the strong oscillation of the response current, while the ZHCs were still operation beyond 2 V, of course with higher i_{leak}.

Based on CV, GCD and potentiostatic aging experiments, we can allude that the compromised operational voltage window of ZHC in CE is in between 0.2 V to 1.8 V, and 0.2 V to 2 V in MCE and WiSE.

Rate Capability of ZHCs. Following the validation of the cell's stable operating voltage range in different electrolytes, their electrochemical behavior was examined further through CV at varying scan rates (as depicted in Figure S22). Qualitatively the following general features can be ascertained from these studies:

(i) The absence of any distinct redox peaks in the CVs suggests that the cell exhibits characteristics similar to those of a classical double-layer capacitor. The preliminary assessment of this double-layer mechanism is sought from the plots of voltammetric current vs. scan rate in logarithmic scale to obtain b-values based on power-law[3] at a representative voltage of 1.4 V for the oxidation and 1 V for the reduction branches of CV traces as illustrated in Figure S23. The voltammogram analysis conducted on

Research Article
doi.org/10.1002/batt.202400414
Chemistry Europe
European Chemical Societies Publishing

various scan rates revealed high b-values ranging from 0.88 to 0.94 in the tested voltage regions, indicating the minimal diffusion-controlled current response and dominance of capacitive-controlled charge storage mechanism.

(ii) Slight deviation from an ideal rectangular CV profiles, particularly at higher scan rates mostly in the case of MCE and WiSE is probably because of Ohmic contributions and/or diffusion-limitations at faster sweep rates.

(iii) It seems the enclosed CV area for CE is higher at faster scan rates, suggesting faster kinetics and thus, better rate capability compared to MCE and WiSE.

Then, GCD was employed to quantify the rate capability of ZHCs. The GCD specific capacitance-voltage curves (in Figure 6a) display typical capacitive behavior, as shown by the linearity of the responses obtained at different current densities, except at 0.05 A g^{-1}. The specific capacitances at various current densities were reported based on the discharge process. It should be noted that both the specific capacitance and the coulombic efficiency for a given current density are not comparable between CE and MCE or WiSE due to different voltage windows being adapted. However, they can be compared between MCE and WiSE. Unlike most of the literature, we normalized the capacitance to the total weight of the self-standing AC buckypaper cathode (AC + SWCNTs + C65), which doesn't contain any binder or metal current collector.

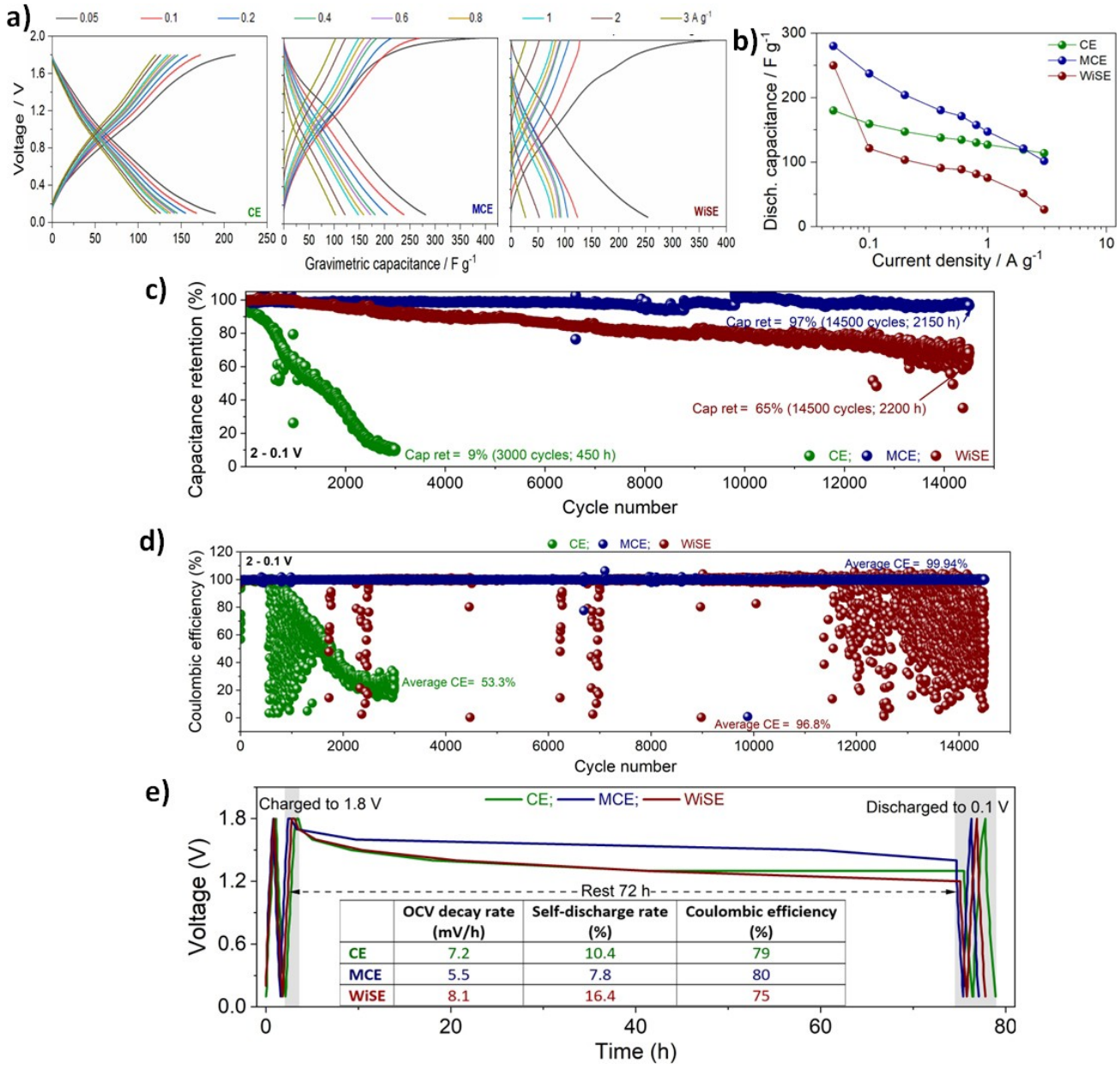

	OCV decay rate (mV/h)	Self-discharge rate (%)	Coulombic efficiency (%)
CE	7.2	10.4	79
MCE	5.5	7.8	80
WiSE	8.1	16.4	75

Figure 6. Electrochemical performance evaluation of ZHCs. a) Rate capability: GCD specific capacitance-voltage profiles at different current densities, and the corresponding capacitances (b). c) Cycling stability tests at 1 A g^{-1} in 2–0.1 V voltage range: % capacity retention, and coulombic efficiencies (d). (e) Self-discharge is evaluated by charging cell to 1.8 V, resting for 72 h, followed by discharging to 0.1 V at 1 A g^{-1}.

Figure 6b and Figure S24a display that a high specific capacitance of approximately 281 $F g^{-1}$ was achieved for MCE at a low current density of 0.05 $A g^{-1}$. However, the capacitance decreases as the current density increases to 0.1, 0.2, 0.4, 0.6, 0.8, 1, 2 and 3 $A g^{-1}$, reaching values of 235, 204, 180, 172, 158, 148, 121 and 102 $F g^{-1}$, respectively. But in the case of WiSE, specific capacitance values were comparably lower at all the current densities, though it was high (252 $F g^{-1}$) at 0.05 $A g^{-1}$. Moreover, as shown in Figure S24b, the coulombic efficiencies remain above 97% at higher current densities (above 0.2 $A g^{-1}$). Understandably, ZHC in CE retained higher capacitances at higher current densities, thus exhibiting the best rate performance retaining 63% at 3 $A g^{-1}$ (in Figure S24c). Nevertheless, at the same current density of 3 $A g^{-1}$, ZHC in MCE retained higher capacitance (36% vs 11%) compared to that in WiSE, indicating better rate performance in our optimized MCE.

Cycle Stability of ZHCs. First, the cycle stability of ZHCs in different electrolytes was carried out using the safe voltage window of 1.8 – 0.1 V at a current density of 1 $A g^{-1}$ (Figure S25). The ZHCs in both MCE and WiSE didn't show any capacity decay upon cycling over 19100 and 15000 cycles, while operational for 2100 and 2400 hours, respectively. But when the CE is used, the capacity retention of ZHC decreased constantly over the cycling until sustained to only 13% after 4000 cycles and 300 hours. Moreover, the MCE also presents the highest average coulombic efficiency of 99.98% compared to 99.96% and 98.7% for WiSE and CE, respectively (Figure S25b). The representative GCD profiles upon cycling are shown in Figure S25c–e, and the most important cycling performance parameters are collected in Table S3.

The cycle stability tests of ZHCs were then considered at the higher voltage range of 2–0.1 V, but using the same current density of 1 $A g^{-1}$ (Figure 6c, d and S26). Once again the results demonstrate that the ZHC in MCE has excellent cyclic stability, with a capacitance retention of 97% even after 14500 cycles and more than 2150 hours (Figure 6c), and an average coulombic efficiency that remains 99.94% throughout the cycling (Figure 6d). However, the capacity retention drops to 9% after only 3000 cycles and 450 hours in the case of CE, while the average coulombic efficiency was only about 53.3%. Even when WiSE is used, the device was not able to match the performances of the MCE-based one. In fact the capacity retention after 14500 cycles and 2200 hours was only 65% with an average coulombic efficiency of 96.8%.

In order to understand the superior cyclability of ZHCs in MCE over CE and WiSE, post-mortem analysis of the cycled cells was carried out. The post-cycled Zn anode in CE showed apparent corrosion pits, cracks, loosely connected dead and porous Zn, along with dendrites (see Figure S27a–c for FE-SEM images). On the other hand, the Zn anode were almost free from these aforementioned detrimental features, still exhibiting almost dendrite-free morphology both in MCE and WiSE (Figure S27d–i). Furthermore, the XRD patterns of the post-cycled Zn anodes were almost similar to the pristine Zn in MCE and WiSE, while that of Zn in CE was dominated by ZnO or zincate species diffraction peaks (Figure S28a).

The surface morphology of post-cycled AC cathode in MCE and WiSE was also similar to that of pristine, retaining its intrinsic porous and well inter-connected particle network characteristics, while in the CE, formation of cracks and severe passivation probably because of by-products deposition was observed (Figure S29). The XRD patterns of the post-cycled AC cathode in MCE and WiSE were identical to the one of the pristine AC, featuring the characteristic broad diffraction peak at 24° corresponding to (002) crystal plane for charge the stored on the surface or in the near-surface of AC (Figure S28b).[49] While in the CE, several new diffraction peaks emerged, along with reduced intensity for the characteristic peak at 24°, once again attesting the by-products deposition observation on the cathode made from FE-SEM analysis.

Self-discharge of ZHCs. Self-discharge characteristics of ZHCs in different electrolytes were compared by monitoring the change of open-circuit voltage (OCV) for a fully charged cell during 72 h of rest period and then discharged to 0.1 V (Figure 6e). Promisingly, the ZHC in MCE exhibited low OCV decay rate of 5.5 vs 7.2%, low self-discharge of 7.8 vs 10.4%, along with slightly higher coulombic efficiency of 80 vs 79% compared to that in CE (Figure S30). Furthermore, these values were also better for ZHC in MCE than in WiSE. The better anti-self-discharge performance in MCE confer that the parasitic reactions (e.g., water electrolysis, corrosion of Zn) are potentially suppressed with the MCE, making it as a promising electrolyte candidate for practical energy storage applications.

Zn//AC vs state-of-the-art ZHCs. The performance of Zn/MCE/AC is compared with state-of-the-art ZHCs (Table S4). However, this comparison is not straightforward due to variations in carbon cathode materials, mass loadings, compositions, electrolyte concentrations, anode thicknesses, and electrochemical testing protocols used in the literature. When similar experimental conditions are available, we compare the performance of Zn/MCE/AC with the state-of-the-art.

Thanks to the high working voltage and moderate specific capacitance, our Zn//AC in MCE delivered a competitive energy density of 138 $Wh kg^{-1}$ at the power density of 44 $Wh kg^{-1}$ and a high power density of 6.5 $kW kg^{-1}$ at the energy density of 17 $Wh kg^{-1}$ (Figure 7a). The energy/power density of our Zn/MCE/AC surpasses most representative ZHCs using concentrated, water-in-salt and MCEs, and is comparable to ZHCs utilizing advanced cathodes with low mass loading (entries 7 and 9; Table S4). As anticipated in the introduction, the energy/power density represents a trade-off between typical Zn batteries and classical capacitors, originating from the hybrid nature of the device.

Yet another stimulating merit of our Zn/MCE/AC is its outstanding cycling stability. Zn/MCE/AC retained ~100 and ~97% of its initial capacity over 19100 and 14500 cycles at 1.8–0.1 V and 2–0.1 V, respectively. Undoubtedly, this excellent cyclability of our device is far better than those tested in similar experimental conditions, for instance at 1 $A g^{-1}$ (Figure 7b).

Research Article
doi.org/10.1002/batt.202400414
Chemistry Europe
European Chemical Societies Publishing

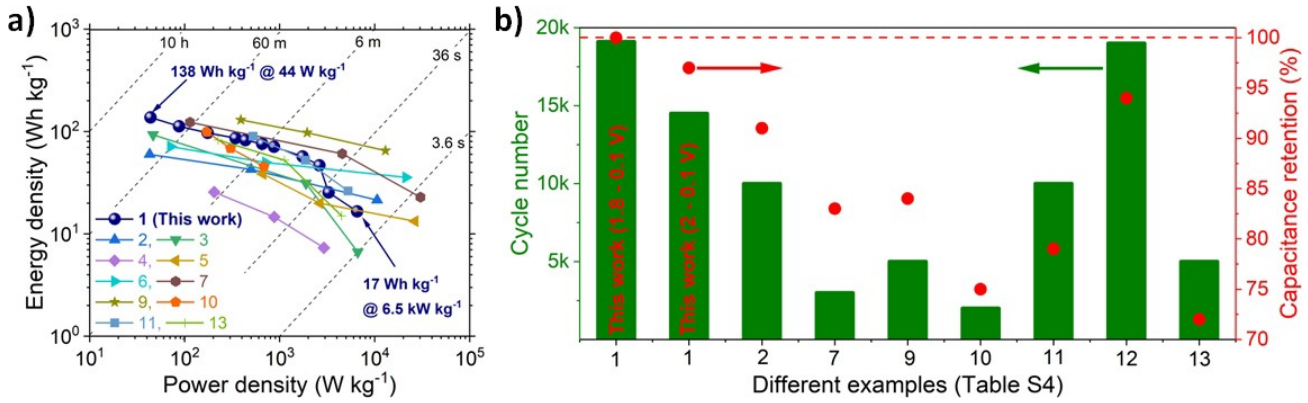

Figure 7. Comparing Zn/MCE/AC electrochemical performance with the state-of-the-art ZHCs. a) Ragone plot. b) Cycle stability showing % capacitance retention and cycle number for different examples collected in Table S4.

Conclusions

In summary, we investigated the stability and reversibility of zinc metal plating/stripping and the performance of Zn//AC full cells in conventional (CE), PEGDME-H_2O (MCE), and water-in-salt (WiSE) aqueous electrolytes. Zinc metal corrodes in CE and WiSE, forming crystalline by-products, but remains almost imperceptible and uniform in MCE. Zn//Cu cells in MCE displayed excellent coulombic efficiencies of 98–100% at various areal capacities and current densities, while asymmetric cells in CE and WiSE had lower efficiencies and became non-operational beyond certain limits of areal capacity and current density. These studies conclude that MCE is superior to CE and WiSE for zinc plating/stripping due to its stability, reversibility, and low parasitic reactions, making it suitable for practical applications. Consequently, both Zn//Cu and Zn//Zn cells in MCE cycled for longer durations than in CE and WiSE. The growth of Zn dendrites, resulting from irregular deposition on the Zn anode and HER, likely led to early cell failure in CE and WiSE, which was substantially delayed with MCE.

The voltage window of the assembled Zn//AC hybrid devices was assessed using CV, GCD, and potentiostatic experiments, revealing an enhanced voltage window of up to 2 V in MCE and WiSE, compared to 1.8 V in CE. ZHC in MCE not only attained the highest capacitance of 281 F g^{-1} (vs. 252 F g^{-1} in WiSE) at 0.05 A g^{-1} but also maintained better rate performance. Impressively, the long-term cyclability of ZHC in MCE was superior to that in CE and WiSE, with better capacity retention and quantitative average coulombic efficiencies. The anti-self-discharge characteristics of ZHC in terms of OCV decay, self-discharge rate, and coulombic efficiency in MCE were also superior to those in CE and WiSE. Finally, the overall performance, particularly cycle stability and energy density, of our hybrid device surpasses most representative ZHCs using concentrated water-in-salt and MCEs. These results suggest that MCE is a promising electrolyte candidate for practical energy storage applications, as it improves Zn anode reactions, consequently resulting in better cell performance.

Experimental Section

Materials

Polyethylene glycol dimethyl ether ($M_n \sim 250$) (PEGDME250) and polyethylene glycol dimethyl ether ($M_n \sim 500$) (PEGDME500) were purchased from Sigma Aldrich, degassed and introduced in a glove box ($O_2 < 0.1$ ppm). 1-Methyl-2-pyrrolidinone (NMP, ACS Reagent, Sigma Aldrich), *iso*-propanol (IPA, Sigma Aldrich) and 1, 5-dichloroanthraquinone (>96%, Sigma Aldrich), were purchased from Sigma Aldrich. Zinc bis(trifluoromethanesulfonyl)imide ($Zn(TFSI)_2$) was synthesized as reported.[50] Zinc (Zn, 99.98%, Alfa Aeser) and Copper (Cu, 99.99%, MTI) foils were polished with sand paper to remove surface oxide layer, washed successively in sonicator with ethanol and milli-Q water, and dried overnight at 60 °C under vacuum. Whatman Grade GF/D Glass Microfiber Filter with 0.67 mm of thickness from Sigma Aldrich was used as separator. Single-walled carbon nanotubes (SWCNTs; Nanografi), LiTFSI (99.9%, Solvionic), commercial activated carbon Picactif BP 10 (AC, PICA), conductive carbon black C65 (TIMCAL).

Methods

Electrolyte Preparation: First, PEGDME450 was prepared by mixing PEGDME 250: PEGDME 500 in the mass ratio of 1:4 as previously reported,[34] degassed and introduced in a glove box. Then, desired amount of degassed deionized water (purified on a MilliQ device from Millipore) was added to PEGDME450 at weight ratio of PEGDME450:H_2O 85:15 inside the argon-filled glove box. Finally, Zn-based molecular crowding electrolyte was prepared by dissolving 1 m (m stands for molality; mol kg^{-1}) of $Zn(TFSI)_2$ ($TFSI^- = [(CF_3SO_2)_2 N]^-$; bis trifluoromethanesulfonimide) in the aforementioned solution and stirred magnetically overnight at room temperature for homogenization. This electrolyte is acronymed as MCE. As a reference, we also prepared a conventional electrolyte of 1 m $Zn(TFSI)_2$ in H_2O without PEGDME450-molecular crowding agent (acronymed as CE) and a well-known water-in-salt electrolyte composed by 1 m $Zn(TFSI)_2$ and 20 m LiTFSI in H_2O (acronymed as WiSE).[21]

AC Electrode Preparation. The self-standing, binder- and metal current collector-free buckypaper AC electrodes were prepared following the modified procedure as previously reported.[37,51] A general procedure to prepare AC electrode with mass loading of 4 mg cm^{-2} is described here. The composition of electrode was fixed to 80:10:10 wt% (AC:C65:SWCNTs). First, 3.7 mg of SWCNTs were dispersed in 20 mL solution of *iso*-propanol (IPA)/*N*-methyl-2-

pyrrolidone (NMP) (1/1 v/v) through a tip sonicator for 10 min (ultrasonic processor UP400S, 400 W, 24 kHz). Then, after 30.3 mg of AC and 3.7 mg of C65 were ball milled together in a Retsch Planetary Ball Mill PM100 (400 rpm, 30 min), those were added to the SWCNTs dispersion and immersed in a bath sonicator (Branson 2510, 100 W, 42 kHz) for 2 h, stirred overnight to prepare the electrode ink. The suspension was filtered through a Nylon membrane filter (47 mm diameter, pore size 0.45 μm) with the help of vacuum, followed by rinsing with IPA. The buckypaper was carefully peeled off from the filter, dried overnight at 70 °C under vacuum, cut into circular discs with a diameter of 10 mm, and directly used as the electrode.

Characterization Methods

Raman spectra of the aqueous electrolytes were recorded with a JASCO NRS-500 Raman equipped with a 534 nm laser, with acquisition time of 15 s and 50 accumulations. The morphology of the Zn and copper substrates and AC cathodes after cycling tests, was observed by field-emission scanning electron microscopy (FE-SEM, JEOL JSM-7900 F) applying 15 kV. The microanalysis was performed by using the Microanalysis Oxford Instrument EDS Ultimmax 170 detector. XRD patterns were recorded by using a PANalitycal Empyream diffractometer with Cu $K_{\alpha;}$ radiation ($\lambda = 1.54178$ Å) at a scanning rate of 0.02° s^{-1}.

Corrosion of Zn: Disks of polished Zn were introduced in a 0.5 mL volume of electrolytes and left for 21 days to soak. Then digital pictures, FE-SEM and XRD were recorded from the cleaned and dried Zn disks.

General Electrochemical Measurements. The ionic conductivity of the aqueous electrolytes was measured by impedance spectroscopy, carried on an electrochemical workstation (Bio-Logic VMP3), in symmetrical coin cells with two stainless steel plate as blocking electrodes (SS//SS) assembled in a glove box. The spectra were recorded in the frequency range of 10^{-1}–10^{6} Hz using a sinusoidal signal with an amplitude of 10 mV at 25 °C at an open circuit voltage (OCV). To confirm the reproducibility of the results, the tests were run on three different replicate cells. The ionic conductivity was calculated by applying the following equation:

$$\sigma = \frac{Cell\ Cost.}{R_b} \tag{1}$$

Where σ (S1 cm^{-1}) is the ionic conductivity, R_b (Ohm^{-1}) is the bulk impedance and it is extracted from the intersection of the Nyquist plot with the real impedance-axis at high frequency, while the cell constant was defined with respect to a standard KCl aqueous solution (1412 μS cm^{-1}).

The Zn transference number ($t_{Zn}{}^{2+}$) measurement was evaluated by DC polarization method, using chronoamperometry in a Zn//Zn symmetrical cell. A polarization voltage of 10 mV was applied across the sample and the initial maximum current I_0 and steady state current I_{SS} were recorded. The Zn^{2+} transference number was calculated by applying the following equation:

$$t_{Zn^{2+}} = \frac{I_0 - I_{SS}}{I_0} \tag{2}$$

The electrochemical stability window of the aqueous electrolytes was explored by linear sweep voltammetry (LSV), using a standard three electrode cell, performed with a Bio-Logic VMP3. The measurements were carried out using platinum as working and Zn as reference and counter electrodes, respectively. LSV tests were realized between the open circuit potential (OCP) and 3 V (*vs* Zn^{2+}/Zn) for the anodic side and −1.5 V (*vs* Zn^{2+}/Zn) for the cathodic side, respectively, at a scan rate of 5 mV s^{-1}. The following Tafel equation has been applied to the anodic sweep branch of LSV to estimate experimental potential dependency of the current density:

$$\eta = a + b\log(i) \tag{3}$$

Where η is the overpotential $(E - E_0)$, i is the current density, and b is the Tafel slope.

The Zn plating/stripping properties were determined by cyclic voltammetry (CV) in a three-electrode configuration with platinum disk (3 mm) as working electrode and Zn foil as both reference and counter electrodes and were performed with a Bio-Logic VMP3 at a scan rate of 1 mV s^{-1}.

The reversibility, cycling, rate performance and Coulombic efficiency measurements of Zn anode were evaluated in Zn//Zn symmetrical and Zn//Cu asymmetrical CR2032 coin-type cells, by galvanostatic charge-discharge (GCD) experiments with a battery testing system Neware (CT-4008–5 V10 mA-164) at 25 °C.

Cell Assembly and Electrochemical Testing

Zn//AC full cells were assembled with AC as cathode, Zn foil as anode and glass fiber (Whatman GF/D) in a CR2032 coin-type cells in the argon filled glove box. The electrolyte was either CE, MCE or WiSE; 125 μL added to the coin cell. The assembled cells were left standing for at least 10 h to insure a proper wetting of cell components, before carrying out electrochemical tests. Unless specifically stated, the electrochemical tests of Zn//AC were carried out with AC cathode mass loading of 4 mg cm^{-2} at room temperature. Cyclic voltammetry at 1 mV s^{-1}, galvanostatic charge-discharge (GCD) at 1 A g^{-1} and potentiostatic aging (2 h) experiments at various upper voltage cut-off limits were carried out at room temperature to evaluate Zn//AC operational voltage window. The CV at different scan rates (v, 0.25–250 mV s^{-1}) was employed to evaluate current-scan rate behavior by power-law analysis.[52,53] The exponential b-value can be determined by the slope of log (i_p) *vs* log (v) plot for the redox processes

$$i_p = av^b \tag{4}$$

where, a and b are adjustable coefficients.

The cycle stability of Zn//AC was carried out at different voltage windows, that are summarized in Table S3. Similarly, rate capability of Zn//AC was also assessed, adapting the requisite voltage window for the particular electrolytes. Both the cycle stability and rate tests were carried out by GCD experiment using a battery testing system Neware (CT-4008-5 V10 mA-164).

The specific capacitance, C (F g^{-1}) was calculated using the following equation:

$$C = \frac{I \times \Delta t}{m \times \Delta V} \tag{5}$$

where I (A) and Δt (s) are discharging current and time, respectively. m (g) is the total mass cathode, including buckypaper components, and ΔV (V) is the working voltage.

The energy density E (Wh kg^{-1}) and power density P (W kg^{-1}) of ZHCs are obtained using following equation:

$$E = \frac{1}{2 \times 3.6} C \Delta V^2 \quad (6)$$

$$P = \frac{E \times 3600}{t} \quad (7)$$

where C (F $g_{cathode+anode}^{-1}$), ΔV (V) and t (s) are the specific capacitance, operational voltage, and discharging time, respectively.

The self-discharge of Zn//AC full cells was investigated by charging and discharging for first ten cycles at 1 A g^{-1}, then charging to 1.8, followed by a rest period (72 h) at OCV, and then discharging at 1 A g^{-1} to 0.1 V. The self-discharge was quantified in terms of OCV decay rate, Coulombic efficiency and self-discharge rate, calculated using the following equation:

$$Self\ discharge\ rate\ \left(\%\frac{1}{h}\right) = \left(\frac{Sp.\ Cap_{cha} - Sp.\ Cap_{disch}}{Sp.\ Cap_{cha}} \times 100\right)/h \quad (8)$$

Where $Sp.\ Cap_{cha}$ is the charge specific capacitance, $Sp.\ Cap_{disch}$ is the discharge specific capacitance obtained immediately after the resting period and h is the rest period in hours.

Supporting Information Summary

Supplementary table and figures are in Supporting Information.

Supporting Information is available from the Wiley Online Library or from the author.

Acknowledgements

Authors thank the Spanish Government; MCIN/AEI/10.13039/501100011033/FEDER "A way of making Europe" (PID2021-124974OB-C21) for the funding. NP appreciates fellowship IJC2020-043076-I-I funded by MCIN/AEI/10.13039/501100011033 and by the European Union NextGenerationEU/PRTR.

Conflict of Interests

The authors declare no conflict of interest.

Data Availability Statement

The data that support the findings of this study are available from the corresponding author upon reasonable request.

Keywords: Aqueous electrolyte · Molecular crowding electrolyte · PEGDME · Self-discharge · Zinc hybrid capacitor

[1] J. Liang, F. Li, H. M. Cheng, *Energy Storage Mater.* **2017**, *7*, A1–A3.
[2] D. Larcher, J.-M. Tarascon, *Nat. Chem.* **2015**, *7*, 19–29.
[3] C. Zhong, Y. Deng, W. Hu, J. Qiao, L. Zhang, J. Zhang, *Chem. Soc. Rev.* **2015**, *44*, 7484–7539.
[4] D. Chao, W. Zhou, F. Xie, C. Ye, H. Li, M. Jaroniec, S.-Z. Qiao, *Sci. Adv.* **2020**, *6*. DOI: 10.1126/sciadv.aba4098.
[5] P. Simon, Y. Gogotsi, *Nat. Mater.* **2008**, *7*, 845–854.
[6] P. H. L. Notten, M. Latroche, *Encycl. Electrochem. Power Sources* **2009**, *4*, 502–521.
[7] F. R. McLarnon, E. J. Cairns, *J. Electrochem. Soc.* **1991**, *138*, 645–656.
[8] H. Pan, Y. Shao, P. Yan, Y. Cheng, K. S. Han, Z. Nie, C. Wang, J. Yang, X. Li, P. Bhattacharya, K. T. Mueller, J. Liu, *Nat. Energy* **2016**, *1*, 16039.
[9] C. Xu, B. Li, H. Du, F. Kang, *Angew. Chem. Int. Ed.* **2012**, *51*, 933–935.
[10] N. Zhang, F. Cheng, Y. Liu, Q. Zhao, K. Lei, C. Chen, X. Liu, J. Chen, *J. Am. Chem. Soc.* **2016**, *138*, 12894–12901.
[11] M. H. Alfaruqi, S. Islam, J. Gim, J. Song, S. Kim, D. T. Pham, J. Jo, Z. Xiu, V. Mathew, J. Kim, *Chem. Phys. Lett.* **2016**, *650*, 64–68.
[12] M. S. Chae, J. W. Heo, S.-C. Lim, S.-T. Hong, *Inorg. Chem.* **2016**, *55*, 3294–3301.
[13] Z. Liu, G. Pulletikurthi, F. Endres, *ACS Appl. Mater. Interfaces* **2016**, *8*, 12158–12164.
[14] M. H. Alfaruqi, J. Gim, S. Kim, J. Song, J. Jo, S. Kim, V. Mathew, J. Kim, *J. Power Sources* **2015**, *288*, 320–327.
[15] H. Li, L. Ma, C. Han, Z. Wang, Z. Liu, Z. Tang, C. Zhi, *Nano Energy* **2019**, *62*, 550–587.
[16] A. A. Mohamad, *J. Power Sources* **2006**, *159*, 752–757.
[17] Y. Li, J. Hu, F. Guan, L. Song, R. Fan, H. Zhu, X. Hu, E. Shen, B. Yang, *Oncol. Rep.* **2013**, *29*, 1805–1810.
[18] Y. Shen, K. Kordesch, *J. Power Sources* **2000**, *87*, 162–166.
[19] F. Wan, L. Zhang, X. Dai, X. Wang, Z. Niu, J. Chen, *Nat. Commun.* **2018**, *9*, 1–11.
[20] K. E. K. Sun, T. K. A. Hoang, T. N. L. Doan, Y. Yu, P. Chen, *Chem. Eur. J.* **2018**, *24*, 1667–1673.
[21] F. Wang, O. Borodin, T. Gao, X. Fan, W. Sun, F. Han, A. Faraone, J. A. Dura, K. Xu, C. Wang, *Nat. Mater.* **2018**, *17*, 543–549.
[22] Z. Zhang, L. Wang, Y. Li, Y. Wang, J. Zhang, G. Guan, Z. Pan, G. Zheng, H. Peng, *Adv. Energy Mater.* **2017**, *7*, 1601814.
[23] N. Choudhary, C. Li, J. Moore, N. Nagaiah, L. Zhai, Y. Jung, J. Thomas, *Adv. Mater.* **2017**, *29*, 1605336.
[24] P. Liu, W. Liu, Y. Huang, P. Li, J. Yan, K. Liu, *Energy Storage Mater.* **2020**, *25*, 858–865.
[25] L. Dong, W. Yang, W. Yang, C. Wang, Y. Li, C. Xu, S. Wan, F. He, F. Kang, G. Wang, *Nano-Micro Lett.* **2019**, *11*, 94.
[26] L. Suo, O. Borodin, T. Gao, M. Olguin, J. Ho, X. Fan, C. Luo, C. Wang, K. Xu, *Science (80-.)* **2015**, *350*, 938–943.
[27] C. Zhang, J. Holoubek, X. Wu, A. Daniyar, L. Zhu, C. Chen, D. P. Leonard, I. A. Rodríguez-Pérez, J. X. Jiang, C. Fang, X. Ji, *Chem. Commun.* **2018**, *54*, 14097–14099.
[28] X. Ji, *eScience* **2021**, *1*, 99–107.
[29] J. Wang, H. Qiu, Z. Zhao, Y. Zhang, J. Zhao, Y. Ma, J. Li, M. Xing, G. Li, G. Cui, *Chem. Res. Chin. Univ.* **2021**, *37*, 328–334.
[30] L. Zhang, I. A. Rodríguez-Pérez, H. Jiang, C. Zhang, D. P. Leonard, Q. Guo, W. Wang, S. Han, L. Wang, X. Ji, *Adv. Funct. Mater.* **2019**, *29*, 1–6.
[31] J. Xie, Z. Liang, Y. C. Lu, *Nat. Mater.* **2020**, *19*, 1006–1011.
[32] D. E. Ciurduc, C. de la Cruz, N. Patil, A. Mavrandonakis, R. Marcilla, *Energy Storage Mater.* **2022**, *53*, 532–543.
[33] M. Peng, L. Wang, L. Li, Z. Peng, X. Tang, T. Hu, K. Yuan, Y. Chen, *eScience* **2021**, *1*, 83–90.
[34] D. Dong, J. Xie, Z. Liang, Y. C. Lu, *ACS Energy Lett.* **2022**, *7*, 123–130.
[35] H. Wang, M. Wang, Y. Tang, *Energy Storage Mater.* **2018**, *13*, 1–7.
[36] L. Dong, X. Ma, Y. Li, L. Zhao, W. Liu, J. Cheng, C. Xu, B. Li, Q.-H. Yang, F. Kang, *Energy Storage Mater.* **2018**, *13*, 96–102.
[37] N. Patil, A. Aqil, F. Ouhib, S. Admassie, O. Inganäs, C. Jérôme, C. Detrembleur, *Adv. Mater.* **2017**, *29*, 1703373.
[38] C. Zhang, J. G. Wang, D. Jin, K. Xie, B. Wei, *Electrochim. Acta* **2015**, *180*, 990–997.
[39] M. Huang, S. Zhen, X. Ren, X. Ju, *J. Power Sources* **2020**, *465*, 228265.
[40] Q. Zhang, Y. Ma, Y. Lu, L. Li, F. Wan, K. Zhang, J. Chen, *Nat. Commun.* **2020**, *11*, 4463.
[41] M. Huang, J. Yang, S. Zhen, C. Wan, X. Jiang, X. Ju, *Chin. Chem. Lett.* **2021**, *32*, 834–837.
[42] J. Pavelec, D. DiGuiseppi, B. Y. Zavlavsky, V. N. Uversky, R. Schweitzer-Stenner, *J. Mol. Liq.* **2019**, *275*, 463–473.
[43] M. Pais, P. Rao, *J. Bio- Tribo-Corrosion* **2019**, *5*, 1–11.
[44] D. Han, S. Wu, S. Zhang, Y. Deng, C. Cui, L. Zhang, Y. Long, H. Li, Y. Tao, Z. Weng, Q. H. Yang, F. Kang, *Small* **2020**, *16*, 1–7.

[45] H. Qiu, X. Du, J. Zhao, Y. Wang, J. Ju, Z. Chen, Z. Hu, D. Yan, X. Zhou, G. Cui, *Nat. Commun.* **2019**, *10*, DOI: 10.1038/s41467-019-13436-3.
[46] M. He, K. Fic, E. Fŗckowiak, P. Novák, E. J. Berg, *Energy Environ. Sci.* **2016**, *9*, 623–633.
[47] X. Zang, C. Shen, M. Sanghadasa, L. Lin, *ChemElectroChem* **2019**, *6*, 976–988.
[48] J. Yang, M. A. Bissett, R. A. W. Dryfe, *ChemSusChem* **2021**, *14*, 1700–1709.
[49] L. F. Aval, M. Ghoranneviss, G. B. Pour, *Heliyon* **2018**, *4*, e00862.
[50] M. J. Earle, U. Hakala, B. J. McAuley, M. Nieuwenhuyzen, A. Ramani, K. R. Seddon, *Chem. Commun.* **2004**, *4*, 1368–1369.
[51] H. Chen, J. Di, Y. Jin, M. Chen, J. Tian, Q. Li, *J. Power Sources* **2013**, *237*, 325–331.
[52] L. E. Blanc, D. Kundu, L. F. Nazar, *Joule* **2020**, *4*, 771–799.
[53] V. Augustyn, J. Come, M. A. Lowe, J. W. Kim, P.-L. Taberna, S. H. Tolbert, H. D. Abruña, P. Simon, B. Dunn, *Nat. Mater.* **2013**, *12*, 518–522.

Manuscript received: June 25, 2024
Revised manuscript received: August 8, 2024
Accepted manuscript online: August 12, 2024
Version of record online: October 4, 2024